

Discovering Quantum Phase Transitions with Fermionic Neural Networks

Gino Cassella^{1,*}, Halvard Sutterud,¹ Sam Azadi,⁴ N. D. Drummond^{1,3}, David Pfau,^{2,1}
James S. Spencer,² and W. M. C. Foulkes¹

¹Department of Physics, Imperial College London, London SW7 2AZ, United Kingdom

²DeepMind, London N1C 4DJ, United Kingdom

³Department of Physics, Lancaster University, Lancaster LA1 4YB, United Kingdom

⁴Department of Physics, University of Oxford, Oxford OX1 3PU, United Kingdom



(Received 28 April 2022; accepted 18 November 2022; published 20 January 2023)

Deep neural networks have been very successful as highly accurate wave function *Ansätze* for variational Monte Carlo calculations of molecular ground states. We present an extension of one such *Ansatz*, FermiNet, to calculations of the ground states of periodic Hamiltonians, and study the homogeneous electron gas. FermiNet calculations of the ground-state energies of small electron gas systems are in excellent agreement with previous initiator full configuration interaction quantum Monte Carlo and diffusion Monte Carlo calculations. We investigate the spin-polarized homogeneous electron gas and demonstrate that the same neural network architecture is capable of accurately representing both the delocalized Fermi liquid state and the localized Wigner crystal state. The network converges on the translationally invariant ground state at high density and spontaneously breaks the symmetry to produce the crystalline ground state at low density, despite being given no *a priori* knowledge that a phase transition exists.

DOI: 10.1103/PhysRevLett.130.036401

The correlated motion of electrons in condensed matter gives rise to rich emergent phenomena. Although these are governed by fundamental quantum mechanical principles known for almost a century, they remain difficult to understand and even harder to predict theoretically or computationally. One of the major themes of modern condensed matter physics is the study of phase transitions caused by electron correlation.

The difficulty of solving the Schrödinger equation scales exponentially with particle number in general, so exact solutions for interacting many-electron systems are rarely accessible. This explains why approximate numerical techniques have become such vital tools in the search for exotic zero-temperature phases, providing accurate predictions of experimentally observable quantities in phases already understood qualitatively. Most computational approaches, however, encode prior assumptions about the appropriate phase, which poses a substantial difficulty in predicting previously unknown electronic states. Changes in symmetry or topology are rarely discovered computationally before they have been seen experimentally or proposed on theoretical grounds.

In this Letter, we introduce a neural-network-based approach to predicting the qualitative nature of electronic ground states in condensed matter. We utilize a representation of the wave function, the fermionic neural network (FermiNet) [1], which is capable of representing *any* antisymmetric state [2], and requires no *a priori* knowledge of the system being studied. Guided by the quantum mechanical variational principle alone, without reference to experimental data, FermiNet can learn the ground state of a many-body interacting Hamiltonian. We extend FermiNet, which has previously only been applied to atoms and molecules [1,3–5], to systems subject to periodic boundary conditions. Phase transitions are seen by studying changes in the ground state as the parameters of the system are varied.

A significant body of recent work has used machine learning to detect phase transitions in simulated classical [6–8] and quantum [9–11] systems, but these studies required a source of external data, looking for patterns characteristic of different phases. Our approach requires only the Hamiltonian. There has also been work using neural network *Ansätze* to study lattice models and spin systems, including their phase transitions [12–16], but for applications to many real systems, the wave function must be treated, as in the present Letter, in continuous space.

The flexibility of FermiNet hinges on the universal approximation property of neural networks [17,18], which makes them a versatile tool for approximating high-dimensional functions and has led to radical advances in

Published by the American Physical Society under the terms of the [Creative Commons Attribution 4.0 International license](#). Further distribution of this work must maintain attribution to the author(s) and the published article's title, journal citation, and DOI.

many computational fields [19–22]. This success has motivated the application of neural networks to solving problems across the physical sciences, including quantum mechanics [12,23–25]. Several neural-network-based wave functions in both first-quantized [1,3,26–28] and second-quantized [29] representations have recently been used to compute the ground-state energies of molecules to a level of accuracy rivaling, or in some cases exceeding, sophisticated quantum chemistry methods such as coupled cluster [30]. FermiNet and *Ansätze* derived from it are the most accurate of these so far, gaining an advantage over second-quantized neural and most quantum chemical approaches because they are basis-set-free. This, coupled with the flexibility of the neural representation, enables the application of FermiNet to generic phases of matter.

We demonstrate the flexibility of the periodic FermiNet by studying the quantum phase transition between the Fermi liquid and Wigner crystal [31] in the three-dimensional interacting homogeneous electron gas (HEG) [32]. Two-dimensional Wigner crystals were very recently imaged for the first time [33–35], but three-dimensional Wigner crystals have not yet been observed in electronic systems and are thus less well understood. The zero-temperature properties of the three-dimensional HEG depend on a single dimensionless parameter r_s defined as the ratio of the radius of a sphere that contains one electron on average to the Bohr radius. At high density (small r_s), the ground state is a weakly interacting Fermi liquid. At low density (large r_s), the correlations are stronger and the translational symmetry breaks spontaneously, giving rise to a spatially ordered Wigner crystal [31].

We find that the same neural network architecture learns the appropriate ground-state wave function either side of the Wigner phase transition, spontaneously breaking continuous translational symmetry when the crystal phase is stable. As we give the network no information about the nature of the ground state, the degree of inductive bias in the determination is very low.

The Hamiltonian for a finite HEG of N electrons subject to periodic boundary conditions is

$$\mathcal{H} = -\frac{1}{2} \sum_{i=1}^N \nabla_i^2 + U_{\text{Coulomb}}, \quad (1)$$

where the indices i label the N electrons in the simulation cell and U_{Coulomb} is the Coulomb energy per simulation cell of an infinite periodic lattice of identical copies of that cell. In practice, the Coulomb energy is evaluated using the Ewald method [36,37]. We work in Hartree atomic units, where energies are measured in hartrees (1 Ha \approx 27.211 eV) and distances in Bohr radii.

The wave function represented by a FermiNet is a sum of determinants of many-electron functions [1,3]:

$$\Psi(\{\mathbf{x}_j\}) = \sum_k^{n_{\text{det}}} \det[\psi_i^k(\mathbf{x}_j; \{\mathbf{x}_{/j}\})], \quad (2)$$

where $\mathbf{x} = (\mathbf{r}, \alpha)$ labels the spatial and spin coordinates of an electron, and the set $\{\mathbf{x}_{/j}\}$ includes all electron coordinates except \mathbf{x}_j . The orbital $\psi_i^k(\mathbf{x}_j; \{\mathbf{x}_{/j}\})$ depends on the coordinates \mathbf{x}_j of the j th electron, and, in a permutation-invariant fashion, on the set of all other electron coordinates. The use of many-electron orbitals makes a FermiNet determinant much more flexible than a Slater determinant of one-electron orbitals, and a linear combination of a small number of FermiNet determinants has a much greater representational capacity than a linear combination of a similar number of Slater determinants [1]. The original FermiNet architecture assumed, as is conventional in variational Monte Carlo (VMC) [38], that the determinants in Eq. (2) can be factorized into spin-up and spin-down determinants. Removing this constraint has proven to be more accurate (see Supplemental Material [39]) and is used here.

FermiNet uses a neural network to approximate the many-electron orbitals appearing in the determinants [1]. The network consists of two parallel streams, for processing one-electron and two-electron information. The one-electron stream is constructed of repeating blocks, where each block contains a nonlinear layer and a permutation-equivariant function. The two-electron stream is a comparatively small fully connected feed-forward network. The outputs of the one- and two-electron streams at each layer are fed into the permutation-equivariant function. The multiple outputs of the one-electron stream are fed through a final linear layer to produce the required number of many-electron functions $\{\phi_i^{ka}\}$. Finally, the network outputs are multiplied by a parametrized envelope \mathbf{f} to produce the many-electron orbitals $\psi_i^{ka}(\mathbf{r}) = f_i^{ka}(\mathbf{r})\phi_i^{ka}(\mathbf{r})$. The electron position vectors \mathbf{r}_i and norms $\|\mathbf{r}_i\|$, and the electron-electron separation vectors $(\mathbf{r}_i - \mathbf{r}_j)$ and norms $\|\mathbf{r}_i - \mathbf{r}_j\|$, are supplied as inputs to the network. Full details of the network architecture are given in Ref. [1] and the Supplemental Material [39].

To adapt the FermiNet architecture to periodic systems, it is sufficient to modify the input features to ensure that periodic boundary conditions are satisfied. Periodic input features are most easily expressed in the basis $\{\mathbf{a}_1, \mathbf{a}_2, \mathbf{a}_3\}$ of primitive Bravais lattice vectors of the simulation cell. For an arbitrary vector, $\mathbf{r} \stackrel{\Delta}{=} s_1 \mathbf{a}_1 + s_2 \mathbf{a}_2 + s_3 \mathbf{a}_3$, the periodic input features are obtained from the fractional coordinates s_i via the componentwise transformation $s_i \rightarrow [\sin(2\pi s_i), \cos(2\pi s_i)]$. A periodic analog of the Euclidean norm may be defined as

$$\begin{aligned} \|s\|_p^2 &= \sum_{ij} [1 - \cos(2\pi s_i)] S_{ij} [1 - \cos(2\pi s_j)] \\ &\quad + \sin(2\pi s_i) S_{ij} \sin(2\pi s_j), \end{aligned} \quad (3)$$

where $S_{ij} = \mathbf{a}_i \cdot \mathbf{a}_j$ acts as a metric tensor in the fractional coordinate system. This definition of the norm is smooth,

TABLE I. Correlation energy of the spin-unpolarized $N = 14$ HEG with simple cubic boundary conditions. The i -FCIQMC energies [41] were calculated using a basis of 778 plane wave orbitals for $r_s = 5.0$ or 2378 plane waves otherwise, corresponding to Hilbert spaces of 10^{24} and 10^{31} Slater determinants, respectively. The extrapolation of i -FCIQMC results to the complete basis set limit may yield correlation energies that are 1–2 mHa too negative [43]. bolded values indicate the lowest energy in each column

Method	Correlation energy (Ha)			
	$r_s = 0.5$	$r_s = 1.0$	$r_s = 2.0$	$r_s = 5.0$
SJB ($n_{\text{det}} = 1$)				
VMC	−0.58624(1)	−0.5254(1)	−0.437(3)	−0.30339(2)
DMC	−0.58778(1)	−0.5254(1)	−0.4385(3)	−0.30474(8)
FermiNet				
$n_{\text{det}} = 1$	−0.58895(6)	−0.52568(3)	−0.43881(1)	−0.30468(1)
$n_{\text{det}} = 16$	−0.59094(6)	−0.52682(3)	−0.44053(1)	−0.30495(1)
i-FCIQMC [41]				
Finite basis	−0.5939(4)	−0.5305(5)	−0.4430(7)	−0.304(1)
Basis set limit	−0.5969(3)	−0.5325(4)	−0.4447(4)	−0.306(1)

periodic with respect to the simulation cell, and proportional to the Euclidean norm as $s \rightarrow 0$. Unlike the simpler norm introduced in Ref. [40], it retains these properties for noncubic simulation cells. Convergence speed and asymptotic convergence are improved by including an envelope of the form

$$f_i^{k\alpha}(\mathbf{r}) = \sum_m [\nu_{im}^{k\alpha} \cos(\mathbf{k}_m \cdot \mathbf{r}) + \mu_{im}^{k\alpha} \sin(\mathbf{k}_m \cdot \mathbf{r})], \quad (4)$$

for real wave functions, or

$$f_i^{k\alpha}(\mathbf{r}) = \sum_m \nu_{im}^{k\alpha} \exp(i\mathbf{k}_m \cdot \mathbf{r}), \quad (5)$$

for complex wave functions. The \mathbf{k}_m are simulation-cell reciprocal lattice vectors up to the Fermi wave vector of the noninteracting electron gas, and $\nu_{im}^{k\alpha}$, $\mu_{im}^{k\alpha}$ are learnable parameters. Finally, when simulating the electron gas, the absence of nuclei (and hence electron-nuclear cusps) removes the need to include the norms of the electron positions as inputs. The FermiNet wave function is optimized using the VMC method [38]. Unless specified, all calculations used the same training procedure and hyperparameters as in Ref. [1]. Further details are given in the Supplemental Material [39].

Table I shows the results of FermiNet calculations of the total energy of a 14-electron simple cubic simulation cell of unpolarized HEG at four different densities. This system is sufficiently small that near-exact initiator full configuration interaction quantum Monte Carlo (i -FCIQMC) benchmarks are available [41,42].

However, the fermion sign problem in FCIQMC increases rapidly with r_s , rendering i -FCIQMC calculations at low densities with large basis sets impractical; the calculations at $r_s = 5$ were $\sim 10^4$ times more expensive than those at $r_s = 1$ [41]. There is no clear systematic trend

with the disagreement between FermiNet and i -FCIQMC; FermiNet is 4–6 mH above i -FCIQMC at $r_s < 5$ and 1 mH above at $r_s = 5$. The variance in the FermiNet energies decreases with r_s ; however, the magnitude of the total energy of the $N = 14$ HEG (see Supplemental Material [39]) also decreases sharply with r_s . As a result, it is ambiguous if the relative accuracy of FermiNet is greater at lower density. Table I also includes VMC and fixed-node diffusion Monte Carlo (DMC) results calculated using a conventional Slater-Jastrow backflow (SJB) wave function.

Although FermiNet is a VMC method, it achieves an accuracy similar to that of SJB DMC, with both approaches obtaining 99% of the i -FCIQMC correlation energy extrapolated to the complete basis set limit (which may be 1–2 mHa too large [43]). FermiNet obtains a similar fraction of the correlation energy for molecular systems with a comparable number of electrons [1]. Again as in molecular systems, calculations using 16 FermiNet determinants are noticeably better than calculations using one FermiNet determinant.

To assess the performance of FermiNet as the strength of the correlation increases, we study the $N = 27$ electron spin-polarized HEG in the density range from $r_s = 1$ to 90 in a body-centered cubic (bcc) cell, as this minimizes the packing density and has the lowest Madelung energy [31] of the Wigner crystal in the low-density limit. Prior work [44,45] had found Wigner crystallization to occur in the interval $r_s = [100, 110]$, although a recent study [46] lowers this estimate substantially. The 27-electron system studied here is very small and there are substantial finite-system-size effects that broaden the phase transition and move it to a much higher density.

Ground-state energies obtained using the VMC method with a FermiNet wave function and using the VMC and DMC methods with SJB wave functions targeted at gas and crystal states are compared in Fig. 1(a) for the 27-electron system. For $r_s \leq 1$, real-valued FermiNets often become trapped in local minima during optimization, with energies

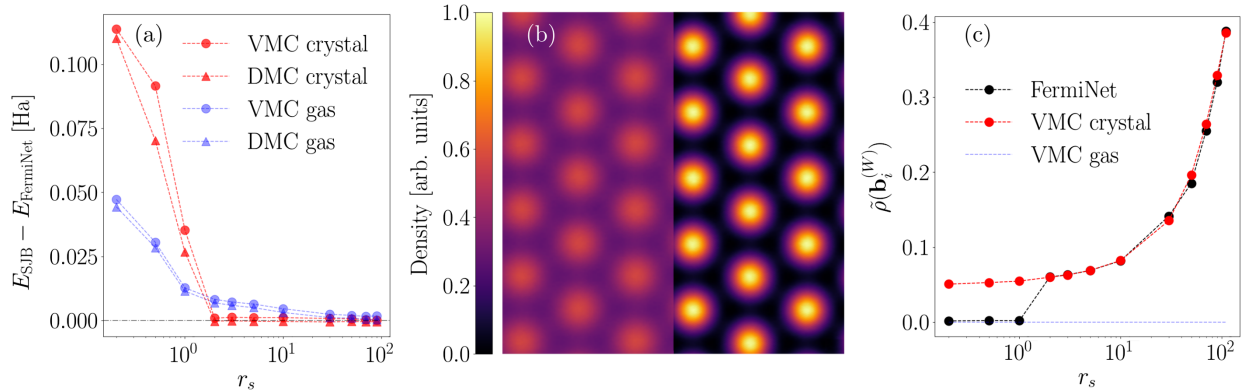


FIG. 1. The $N = 27$ spin-polarized homogeneous electron gas in a body-centered cubic (bcc) simulation cell. (a) Single-determinant Slater-Jastrow backflow (SJB) ground-state total energies per electron relative to FermiNet. The “gas” and “crystal” results were obtained using SJB wave functions built using determinants of plane waves and Gaussian orbitals, respectively. Error bars are smaller than the markers. FermiNet results for $r_s \leq 1$ used complex wave functions. the FermiNet VMC method yields a variational improvement over the SJB VMC and SJB DMC method results in the gas phase and over the SJB VMC method results in the crystal phase. (b) One-electron density from the FermiNet VMC method at $r_s = 10$ (left) and 70 (right), projected into the (011) plane of the conventional bcc structure. Four simulation cells are shown. Length scales are normalized by r_s , such that the apparent length scales are equivalent and crystal sites are superimposable. (c) Order parameter averaged over crystal axes for the bcc Wigner crystal state. Error bars are smaller than the markers. At small values of r_s , the order parameter is ~ 0 , corresponding to a uniform one-electron density (gaslike); the order parameter rises sharply to a finite value at $r_s = 2$, corresponding to the emergence of a crystalline state.

typically $\sim 0.1\%$ higher than the SJB DMC benchmarks. Complex-valued FermiNets do not become trapped in local minima at these densities, and converge to wave functions with a uniform-in-space complex phase, indicating that a complex wave function improves optimization, rather than simply increasing representational capacity. All other results were obtained with real wave functions. The SJB *Ansätze* used to describe gases and crystals are detailed in the Supplemental Material [39] and Ref. [45]. FermiNet VMC calculations produce a tighter variational lower bound than both the SJB gas and crystal wave functions at all densities. Furthermore, FermiNet outperforms fixed-node DMC calculations based on a SJB gas wave function across the entire density range, even at $r_s \leq 1$. In the low-density regime, fixed-node DMC calculations using the SJB crystal wave function give slightly better results than our FermiNet VMC calculations. These results suggest that the nodal surface of the SJB crystal wave function is highly accurate but that the shape of the wave function away from the nodal surface is captured better by FermiNet. Figure 1(b) shows scans of the one-electron density of FermiNet wave functions at $r_s = 10$ and 70 in the $(\mathbf{a}_2, \mathbf{a}_3)$ plane, which is normal to the (011) direction of the conventional bcc cell. Figure 1(c) shows the Fourier component of the one-electron density $\tilde{\rho}$ (see Supplemental Material [39]), an order parameter appropriate for the Wigner crystal, as calculated from VMC simulations using FermiNet and SJB gas and crystal wave functions. These results show that FermiNet is capable of learning wave functions in both the gas and Wigner crystal states to very high accuracy without any handcrafted features indicating whether the wave function should be localized or diffuse, any specific

designation of crystal sites, or any other information that a transition should occur. Unlike the gas and crystal SJB trial wave functions required to describe the gaseous and crystalline states accurately, the FermiNet *Ansatz* is identical across the entire density range.

The HEG Hamiltonian is symmetric under the simultaneous translation of all electron coordinates. Thus, the true ground state of the Wigner crystal is uniform in the one-electron density, with the crystal appearing only in the pair-correlation function. This is known as a “floating crystal” state [47,48]. In Refs. [45,46], it is shown that the energy difference between the fixed and floating crystal is approximately $\Delta E = 0.055r_s^{-3/2}$. While FermiNet differs from Slater-type wave functions used to derive ΔE , we expect a similar reduction in kinetic energy. At low r_s , ΔE is large (20 mHa at $r_s = 2$), so we would expect FermiNet to learn the floating crystal state. Figures 1(b) and 1(c) show that FermiNet instead learns the fixed crystal. The notion of a fixed origin can be removed by removing the one-electron features; however, we find this increases the energy obtained. This suggests that the two-electron stream is insufficiently flexible to fully describe the two-electron correlations in the Wigner crystal without help from the one-electron stream. Improving the flexibility of the two-electron stream will be the focus of future work. We do not believe that these issues impact the central conclusion of the present Letter, and stress that in real condensed matter systems the Hamiltonian does not possess continuous translational symmetry.

Other recent works have explored using neural networks to represent wave functions in real-space periodic systems. Pescia *et al.* use a DeepSets architecture to study bosons in

1D and 2D, obtaining results competitive with conventional DMC result [40]. The iterative backflow network approach of Holzmann and co-workers [49–51] represents Jastrow and backflow functions in a manner equivalent to fully connected neural networks. They observe liquid and solid phases of 2D (bosonic) ^4He [50], but the application to the HEG [51] gives a higher energy at low density than the crystal state observed by Drummond *et al.* [45]. Recently, two related works have been reported. Wilson *et al.* presented FermiNet-based and iterative backflow results for the 14-electron system studied here, plus 7- and 19-electron HEGs [52]. Although they used a more heavily modified version of the FermiNet architecture and include a backflow-based term in the orbitals, their results are similar to ours. Li *et al.* used a similar but smaller FermiNet architecture to ours, with simpler periodic inputs and no envelope function, to study the $N = 54$ HEG along with other atomic solids [53], but do not outperform their SJB VMC or DMC baseline energies. Neither of these two works address Wigner crystallization. We expect that other FermiNet-derived models are capable of discovering phase transitions, as in the present Letter; however, we are unsure if this applies to the heavily modified *Ansatz* of Wilson *et al.* which introduces a higher degree of inductive bias via the inclusion of Hartree-Fock orbitals in the determinant. Applying any of the aforementioned approaches to fermionic systems, including FermiNet, incurs the same $\mathcal{O}(N^3)$ scaling of determinant evaluation. An additional factor of N is introduced if analytic gradients are not available and the Laplacian must be evaluated via automatic differentiation.

To summarize, we have extended the FermiNet neural wave function to calculations with periodic boundary conditions. This we accomplished by making minimal, physically motivated, modifications to render the input features periodic, and by adding a periodic envelope function. As proof of concept, we have demonstrated the accuracy of the modified architecture on the $N = 14$ HEG, where we obtained ~99% of the correlation energy and slightly outperformed VMC and DMC calculations using conventional one-determinant SJB trial wave functions. For the $N = 27$ HEG, we see that FermiNet is capable of learning the localized Wigner crystal phase *a priori*, producing energies in excellent agreement with SJB trial wave functions which encode the qualitative nature of the ground state in their construction. This suggests that FermiNet may be capable of determining novel quantum phases in condensed matter given only the Hamiltonian.

To study quantum phase transitions in realistic strongly correlated electronic systems, it will be necessary to scale to larger numbers of electrons to overcome finite-size effects. However, the scaling required to achieve a fixed accuracy per electron is not yet known. Achieving an acceptable accuracy at an affordable scaling may require additional innovations in the neural network architecture employed. FermiNet could

also be used as a trial wave function for DMC calculations in periodic boundary conditions, an approach that yields small improvements in molecular systems [4]. More generally, we believe that the flexibility and accuracy offered by neural networks make them promising tools for studying complex correlation effects and other emergent phenomena. The advantages of neural-network-based methods are most compelling when the phenomena in question are unexpected or not yet understood.

This work was undertaken with funding from the UK Engineering and Physical Sciences Research Council (EP/T51780X/1) (G. C.) and the Aker scholarship (H. S.). Calculations were carried out with resources provided by the Baskerville Accelerated Compute Facility through a UK Research and Innovation Access to HPC grant. Via his membership of the UK’s HEC Materials Chemistry Consortium, which is funded by EPSRC (EP/R029431), W. M. C. F. used the UK Materials and Molecular Modelling Hub for computational resources, MMM Hub, which is partially funded by EPSRC (EP/T022213). Our SJB DMC Wigner crystal calculations were performed using Lancaster University’s High-End Computing cluster, and the ARCHER2 UK National Supercomputing Service [54] via our membership of the UKs HEC Materials Chemistry Consortium, which is funded by EPSRC (EP/R029431).

*g.cassella20@imperial.ac.uk

- [1] D. Pfau, J. S. Spencer, A. G. D. G. Matthews, and W. M. C. Foulkes, *Phys. Rev. Res.* **2**, 033429 (2020).
- [2] M. Hutter, [arXiv:2007.15298](https://arxiv.org/abs/2007.15298).
- [3] J. S. Spencer, D. Pfau, A. Botev, and W. M. C. Foulkes, [arXiv:2011.07125](https://arxiv.org/abs/2011.07125).
- [4] M. Wilson, N. Gao, F. Wudarski, E. Rieffel, and N. M. Tubman, [arXiv:2103.12570](https://arxiv.org/abs/2103.12570).
- [5] X. Li, C. Fan, W. Ren, and J. Chen, *Phys. Rev. Res.* **4**, 013021 (2022).
- [6] L. Wang, *Phys. Rev. B* **94**, 195105 (2016).
- [7] J. Carrasquilla and R. G. Melko, *Nat. Phys.* **13**, 431 (2017).
- [8] E. P. Van Nieuwenburg, Y.-H. Liu, and S. D. Huber, *Nat. Phys.* **13**, 435 (2017).
- [9] S. Arai, M. Ohzeki, and K. Tanaka, *J. Phys. Soc. Jpn.* **87**, 033001 (2018).
- [10] J. Venderley, V. Khemani, and E.-A. Kim, *Phys. Rev. Lett.* **120**, 257204 (2018).
- [11] Y. Zhang, A. Mesaros, K. Fujita, S. D. Edkins, M. H. Hamidian, K. Chng, H. Eisaki, S. Uchida, J. C. S. Davis, E. Khatami, and E.-A. Kim, *Nature (London)* **570**, 484 (2019).
- [12] G. Carleo and M. Troyer, *Science* **355**, 602 (2017).
- [13] H. Saito, *J. Phys. Soc. Jpn.* **86**, 093001 (2017).
- [14] D. Luo and B. K. Clark, *Phys. Rev. Lett.* **122**, 226401 (2019).
- [15] J. Stokes, J. R. Moreno, E. A. Pnevmatikakis, and G. Carleo, *Phys. Rev. B* **102**, 205122 (2020).

- [16] N. Astrakhantsev, T. Westerhout, A. Tiwari, K. Choo, A. Chen, M. H. Fischer, G. Carleo, and T. Neupert, *Phys. Rev. X* **11**, 041021 (2021).
- [17] G. Cybenko, *Math. Control Signal Syst.* **2**, 303 (1989).
- [18] K. Hornik, *Neural Netw.* **4**, 251 (1991).
- [19] A. Krizhevsky, I. Sutskever, and G. E. Hinton, *NeurIPS 25* (2012).
- [20] A. Vaswani, N. Shazeer, N. Parmar, J. Uszkoreit, L. Jones, A. N. Gomez, L. u. Kaiser, and I. Polosukhin, in *Advances in Neural Information Processing Systems*, edited by I. Guyon, U. V. Luxburg, S. Bengio, H. Wallach, R. Fergus, S. Vishwanathan, and R. Garnett (Curran Associates, Inc., 2017), Vol. 30.
- [21] D. Silver, A. Huang, C. J. Maddison, A. Guez, L. Sifre, G. Van Den Driessche, J. Schrittwieser, I. Antonoglou, V. Panneershelvam, M. Lanctot *et al.*, *Nature (London)* **529**, 484 (2016).
- [22] J. Jumper, R. Evans, A. Pritzel, T. Green, M. Figurnov, O. Ronneberger, K. Tunyasuvunakool, R. Bates, A. Žídek, A. Potapenko *et al.*, *Nature (London)* **596**, 583 (2021).
- [23] G. Torlai, G. Mazzola, J. Carrasquilla, M. Troyer, R. Melko, and G. Carleo, *Nat. Phys.* **14**, 447 (2018).
- [24] R. G. Melko, G. Carleo, J. Carrasquilla, and J. I. Cirac, *Nat. Phys.* **15**, 887 (2019).
- [25] K. T. Schütt, S. Chmiela, O. A. von Lilienfeld, A. Tkatchenko, K. Tsuda, and K.-R. Müller, *Lect. Notes Phys.* (2020).
- [26] J. Hermann, Z. Schätzle, and F. Noé, *Nat. Chem.* **12**, 891 (2020).
- [27] M. Scherbela, R. Reisenhofer, L. Gerard, P. Marquetand, and P. Grohs, *arXiv:2105.08351*.
- [28] N. Gao and S. Günemann, *arXiv:2110.05064*.
- [29] K. Choo, A. Mezzacapo, and G. Carleo, *Nat. Commun.* **11**, 2368 (2020).
- [30] I. Shavitt and R. J. Bartlett, *Many-Body Methods in Chemistry and Physics: MBPT and Coupled-Cluster Theory*, Cambridge Molecular Science (Cambridge University Press, Cambridge, England, 2009).
- [31] E. Wigner, *Phys. Rev.* **46**, 1002 (1934).
- [32] G. Giuliani and G. Vignale, *Quantum Theory of the Electron Liquid* (Cambridge University Press, Cambridge, England, 2005).
- [33] Y. Zhou, J. Sung, E. Brutschea, I. Esterlis, Y. Wang, G. Scuri, R. J. Gelly, H. Heo, T. Taniguchi, K. Watanabe *et al.*, *Nature (London)* **595**, 48 (2021).
- [34] T. Smoleński, P. E. Dolgirev, C. Kuhlenkamp, A. Popert, Y. Shimazaki, P. Back, X. Lu, M. Kroner, K. Watanabe, T. Taniguchi *et al.*, *Nature (London)* **595**, 53 (2021).
- [35] H. Li, S. Li, E. C. Regan, D. Wang, W. Zhao, S. Kahn, K. Yumigeta, M. Blei, T. Taniguchi, K. Watanabe *et al.*, *Nature (London)* **597**, 650 (2021).
- [36] P. Ewald, *Ann. Phys. (N.Y.)* **369**, 253 (1921).
- [37] L. M. Fraser, W. M. C. Foulkes, G. Rajagopal, R. J. Needs, S. D. Kenny, and A. J. Williamson, *Phys. Rev. B* **53**, 1814 (1996).
- [38] W. M. C. Foulkes, L. Mitas, R. J. Needs, and G. Rajagopal, *Rev. Mod. Phys.* **73**, 33 (2001).
- [39] See Supplemental Material at <http://link.aps.org/supplemental/10.1103/PhysRevLett.130.036401> for a detailed overview of the neural network architecture used in our calculations, details of the Slater-Jastrow-Backflow wavefunctions used for benchmarking, and various data tables used to produce the results in the main text.
- [40] G. Pescia, J. Han, A. Lovato, J. Lu, and G. Carleo, *Phys. Rev. Res.* **4**, 023138 (2022).
- [41] J. J. Shepherd, G. H. Booth, and A. Alavi, *J. Chem. Phys.* **136**, 244101 (2012).
- [42] D. Cleland, G. H. Booth, and A. Alavi, *J. Chem. Phys.* **134**, 024112 (2011).
- [43] V. A. Neufeld and A. J. W. Thom, *J. Chem. Phys.* **147**, 194105 (2017).
- [44] D. M. Ceperley and B. J. Alder, *Phys. Rev. Lett.* **45**, 566 (1980).
- [45] N. D. Drummond, Z. Radnai, J. R. Trail, M. D. Towler, and R. J. Needs, *Phys. Rev. B* **69**, 085116 (2004).
- [46] S. Azadi and N. D. Drummond, *Phys. Rev. B* **105**, 245135 (2022).
- [47] R. F. Bishop and K. H. Lührmann, *Phys. Rev. B* **26**, 5523 (1982).
- [48] M. Lewin, E. H. Lieb, and R. Seiringer, *Phys. Rev. B* **100**, 035127 (2019).
- [49] M. Taddei, M. Ruggeri, S. Moroni, and M. Holzmann, *Phys. Rev. B* **91**, 115106 (2015).
- [50] M. Ruggeri, S. Moroni, and M. Holzmann, *Phys. Rev. Lett.* **120**, 205302 (2018).
- [51] M. Holzmann and S. Moroni, *Phys. Rev. Lett.* **124**, 206404 (2020).
- [52] M. Wilson, S. Moroni, M. Holzmann, N. Gao, F. Wudarski, T. Vegge, and A. Bhownik, *arXiv:2202.04622*.
- [53] X. Li, Z. Li, and J. Chen, *arXiv:2203.15472*.
- [54] <http://www.archer2.ac.uk>.